Science Advances
AAAS

advances.sciencemag.org/cgi/content/full/7/2/eabd4413/DC1

Supplementary Materials for

Structural basis for the regulation of nucleosome recognition and HDAC activity by histone deacetylase assemblies

Jung-Hoon Lee*, Daniel Bollschweiler, Tillman Schäfer, Robert Huber*

*Corresponding author. Email: hlee@biochem.mpg.de (J.-H.L.); huber@biochem.mpg.de (R.H.)

Published 8 January 2021, *Sci. Adv.* **7**, eabd4413 (2021)
DOI: 10.1126/sciadv.abd4413

This PDF file includes:

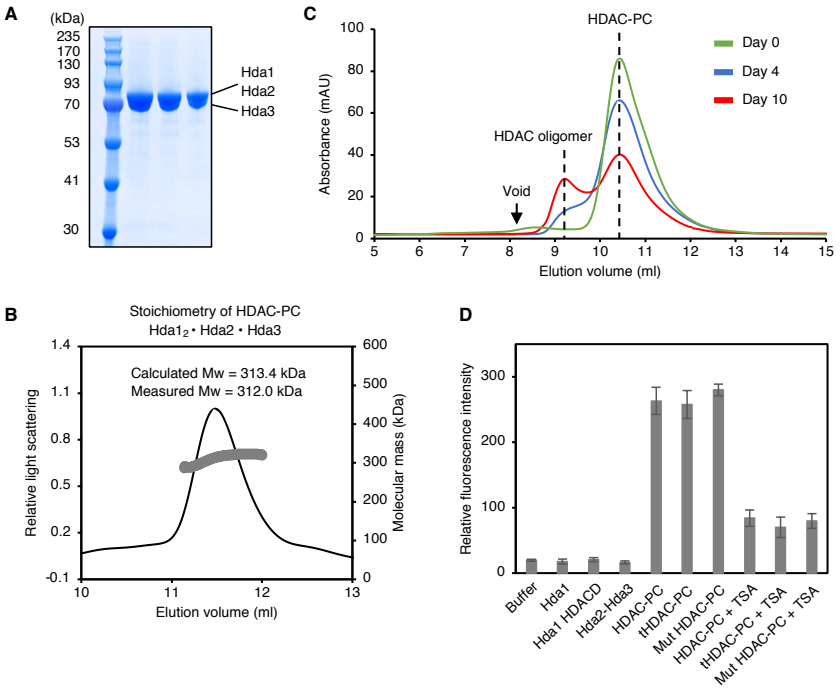

Fig. S1. Biochemical analysis of *S. cerevisiae* class II HDAC complex. (**A**) SDS-PAGE of purified HDAC-PC for cryo-EM grid preparation. (**B**) SEC-MALS analysis of HDAC-PC. (**C**) SEC analysis of purified HDAC-PC showing a progressive oligomerization of the HDAC complex over time. (**D**) *In vitro* deacetylase activities of various purified proteins. All data from three separate measurements were averaged, and the error bars correspond to the standard deviations of the three experiments. Hda1 HDACD = Hda1 1-436, tHDAC-PC = (Hda1 1-436)$_2$-Hda2-Hda3, Mut HDAC-PC = Hda1$_2$ K664A/R666A/K667A/K668A-Hda2 K216A-Hda3 K98A/R103A/K166A/K168A/Q169A/K170A.

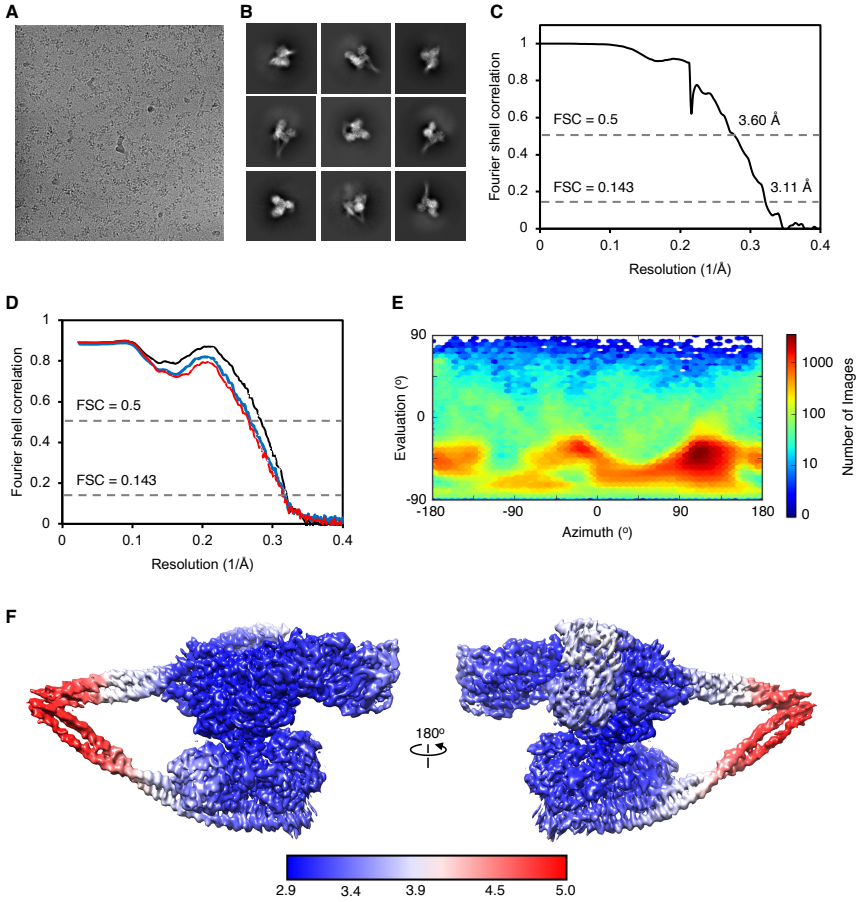

Fig. S2. Cryo-EM analysis of *S. cerevisiae* class II HDAC-PC. (**A**) Representative raw particles from an original micrograph. (**B**) Representative reference-free 2D class averages of HDAC-PC. (**C**) Gold-standard FSC curve for the density map. The overall resolution is estimated at 3.11 Å (FSC = 0.143). (**D**) Model map FSC curve calculated between the refined atomic model and the half map used for refinement (blue, FSC_{work}), the second half-map not used in refinement (red, FSC_{test}) and the full map (black, FSC_{full}). (**E**) Heat map showing particle orientation distribution. (**F**) Local resolution represented by a heat map on the density contour (unsharpened, summed map).

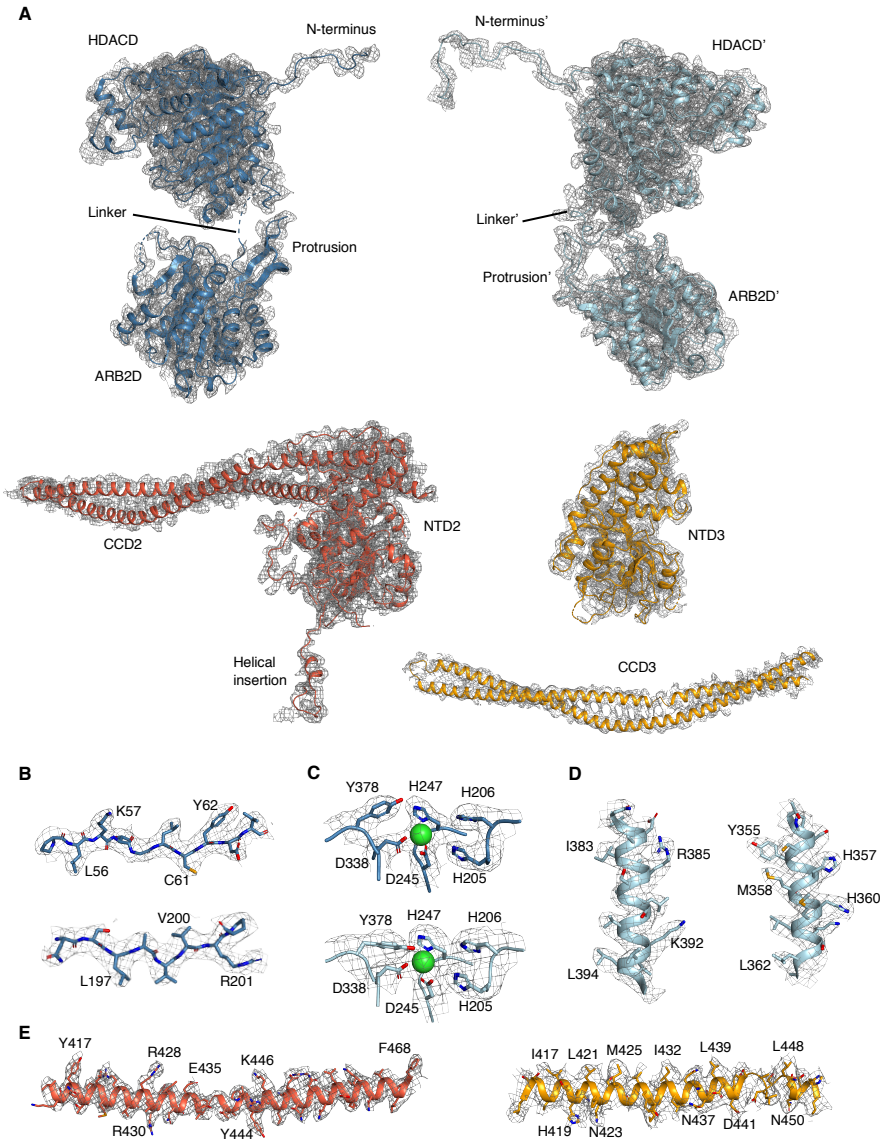

Fig. S3. 3.11 Å resolution cryo-EM maps of HDAC-PC. (**A**) EM density map and the atomic model are shown for all three subunits (individual Hda1 chains in steel blue and light blue, Hda2 in red, and Hda3 in orange). **(B)** Representative EM density maps and the atomic models are shown for one Hda1 chain, **(C)** the active sites of the Hda1 dimer, (**D**) parts of the other Hda1 chain, **(E)** CCD2 of Hda2 in red, and CCD3 of Hda3 in orange.

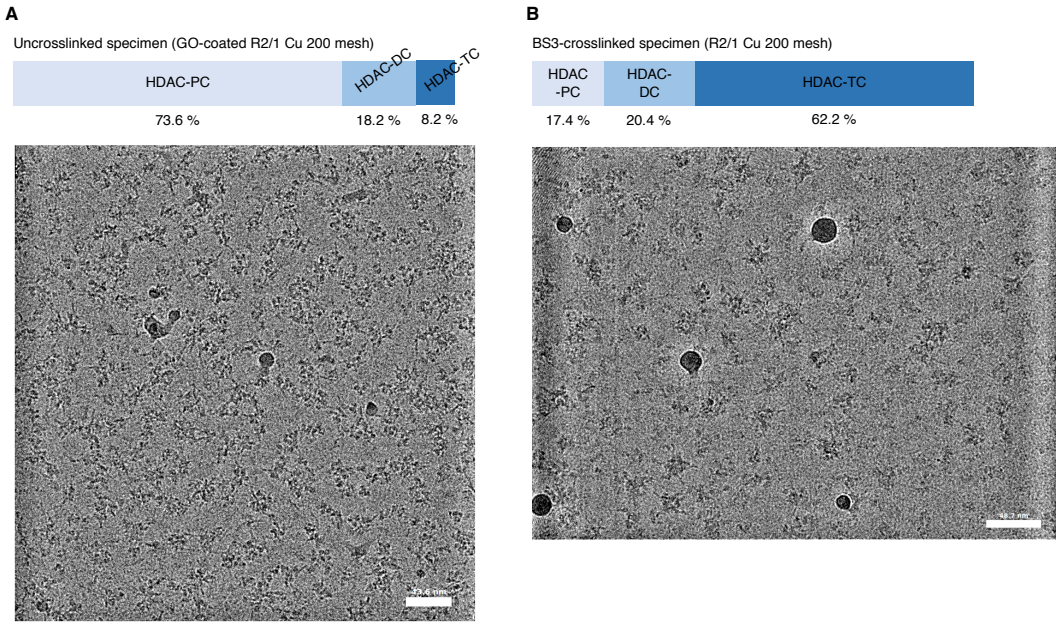

Fig. S4. Change of three subpopulations of HDAC complexes upon chemical crosslinking. **(A)** 2D classification of cryo-EM images acquired with uncrosslinked and **(B)** BS3-crosslinked specimens revealed shifts in subpopulations upon the chemical crosslinking.

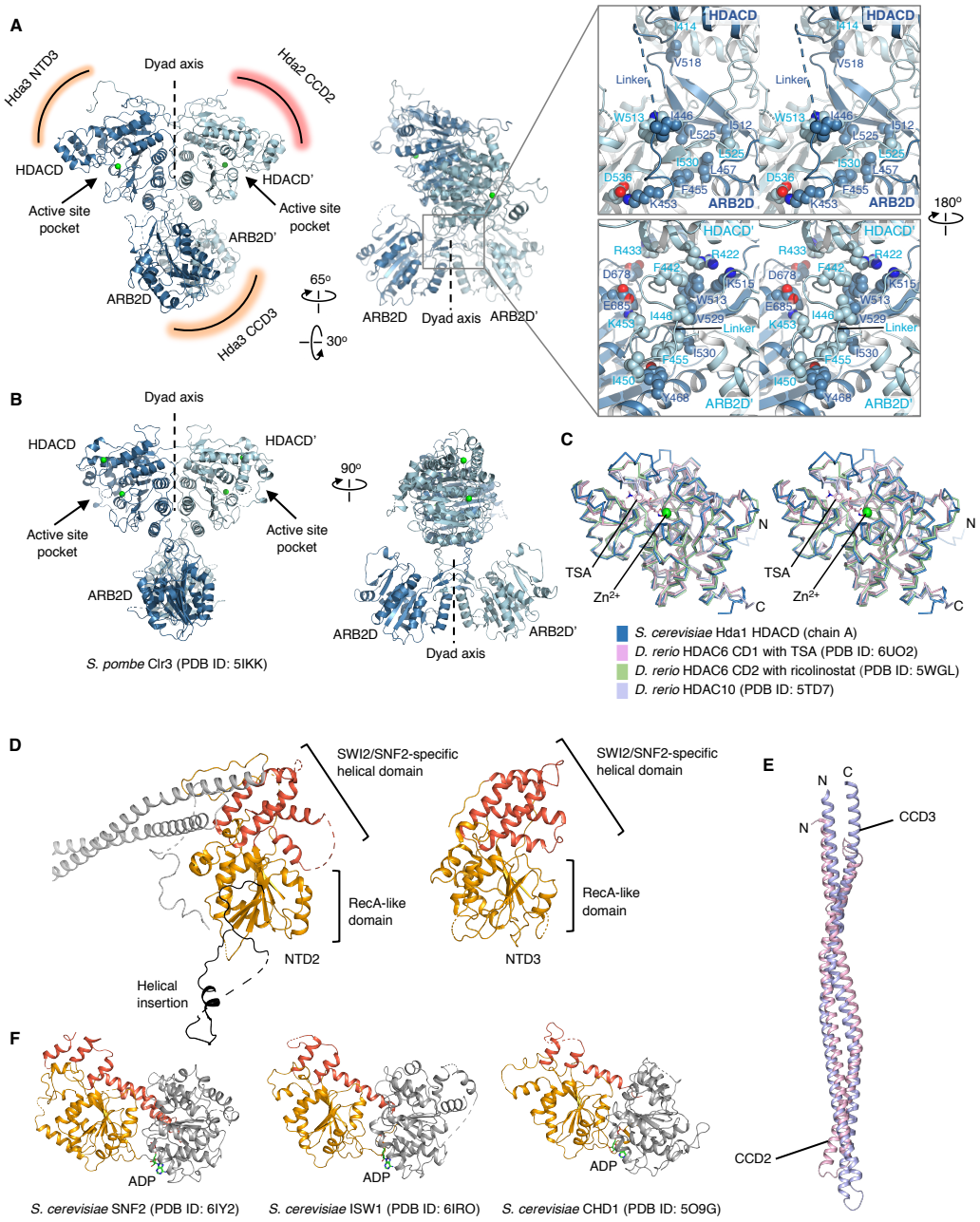

Fig. S5. Structural comparison of HDAC-PC components with other class II HDACs and ATP-dependent chromatin remodelers. (**A**) Two views of a cartoon representation of the Hda1 dimer observed in HDAC-PC (left) and close-up views in stereo of the interfaces between HDACD and ARB2Ds (right). (**B**) Crystal structure of *S. pombe* Clr3 (*11*). (**C**) Superposition in stereo of the Hda1 HDACD with mammalian class II HDAC6 (*12, 13*) and HDAC10 (*42*). (**D**) Structural comparison of the N-terminal halves and (**E**) C-terminal CCDs of Hda2 and Hda3. (**F**) The second helicase lobes of three chromatin remodelers (*43-45*) resemble NTD2 and NTD3.

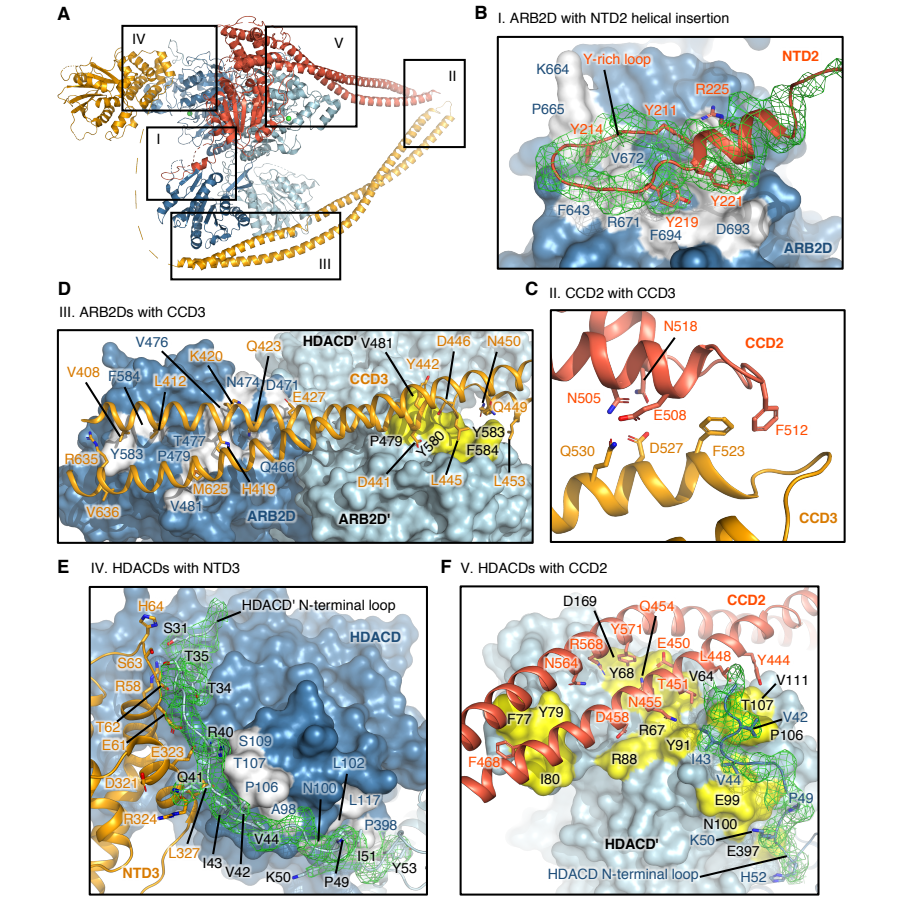

Fig. S6. Recognition interfaces between HDAC-PC components. (**A-F**) Magnified views of key interfaces in HDAC-PC. (**G**) The amino acid conservation in the interfaces between HDACD and CCD2/NTD3 of *S. cerevisiae* and two pathogenic *Candida* species.

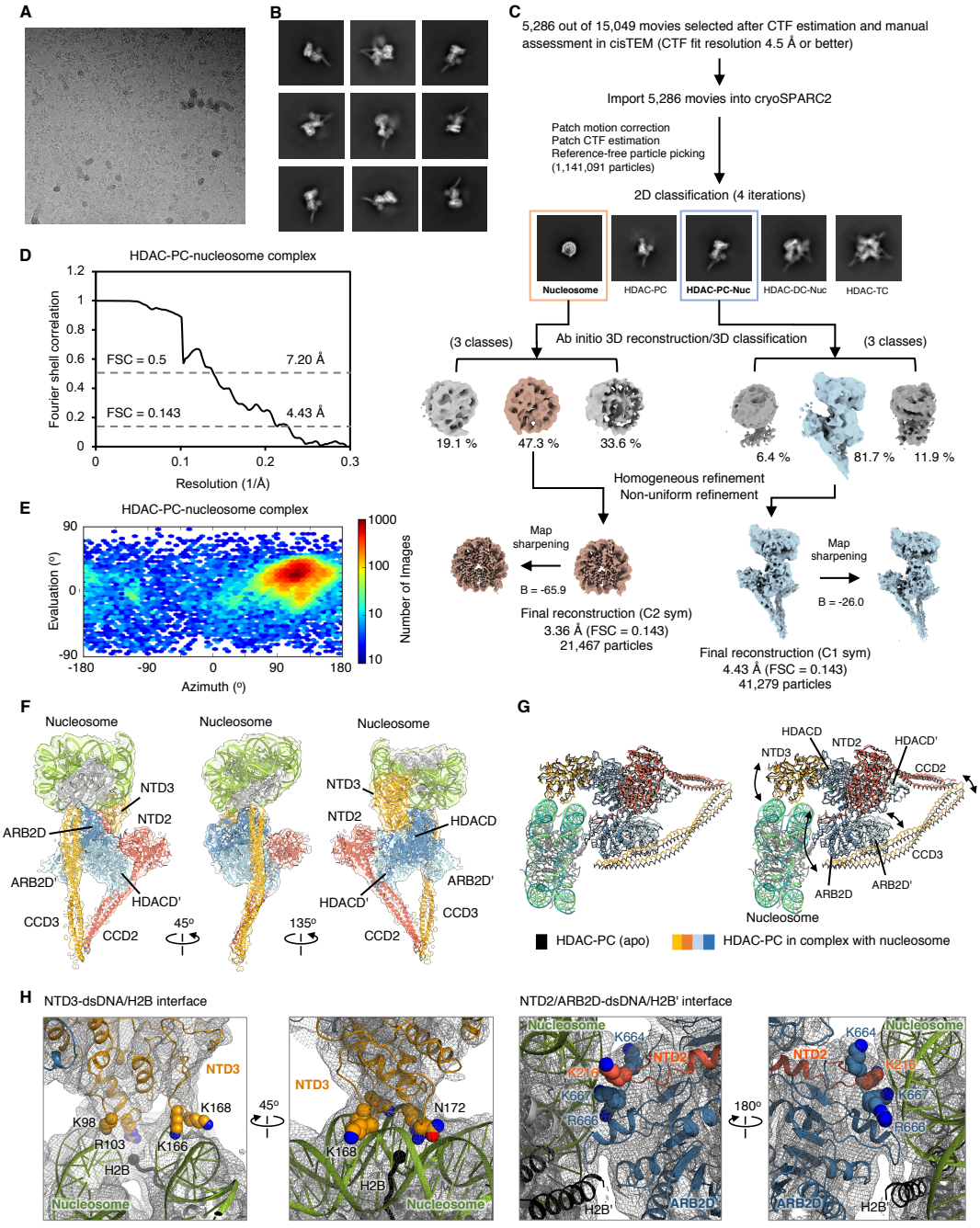

Fig. S7. Cryo-EM analysis of HDAC-PC in complex with nucleosome. (**A**) Representative micrograph. (**B**) Representative 2D classes of HDAC-PC bound to nucleosome. (**C**) Summary of the image processing workflow. (**D**) Gold-standard FSC curve for the density map of HDAC-PC-nucleosome complex. (**E**) Heat map showing particle orientation distribution. (**F**) Three views of the 4.43 Å resolution cryo-EM map of HDAC-PC-nucleosome complex with fitted coordinate. (**G**) Superposition in stereo of HDAC-PC with and without nucleosome. Substantial domain movements are indicated by arrows. (**H**) Close-up views of the interfaces between HDAC-PC and nucleosome fitted into 4.43 Å resolution cryo-EM map.

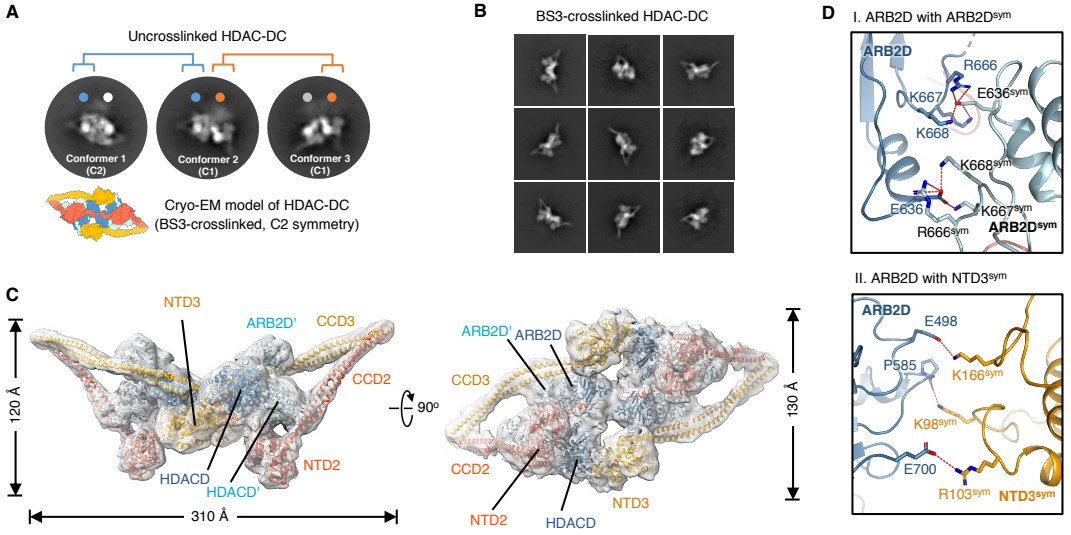

Fig. S8. Cryo-EM analysis of *S. cerevisiae* class II HDAC-DC. (A) Representative 2D class averages of the uncrosslinked HDAC-DC. The same orientation of HDAC-PC observed in the three conformers is colored in blue or orange. Cryo-EM structure of BS3-crosslinked HDAC-DC is shown for comparison (bottom). **(B)** Representative 2D class averages of BS3-crosslinked HDAC-DC. **(C)** Two orthogonal views of HDAC-DC fitted into 8.55 Å resolution cryo-EM map. **(D)** Close-up views of two dimerization interfaces.

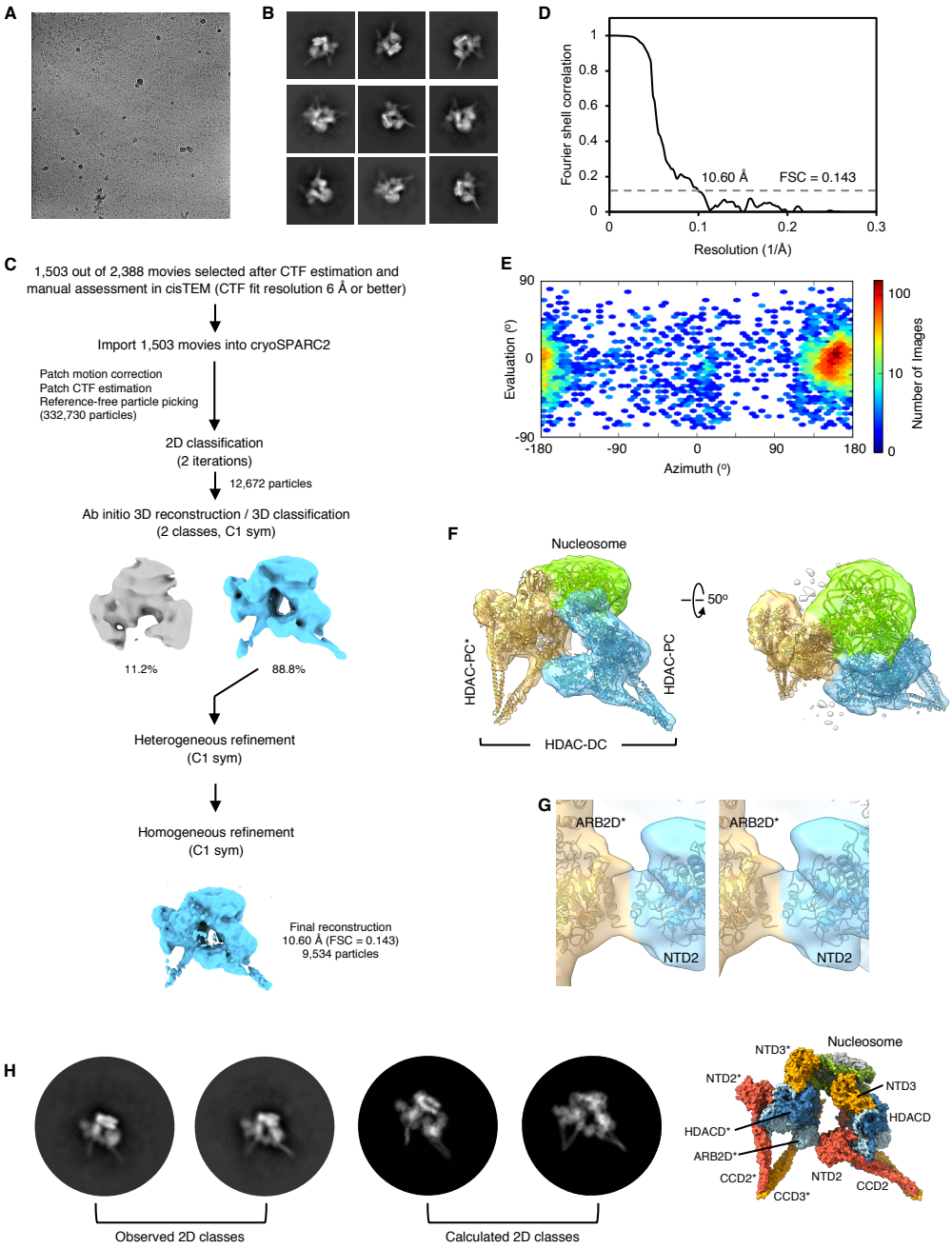

Fig. S9. Cryo-EM analysis of HDAC-DC in complex with nucleosome. (**A**) Representative micrograph. (**B**) Representative 2D classes of HDAC-DC bound to nucleosome. (**C**) Summary of the image processing workflow. (**D**) Gold-standard FSC curve for the density map of HDAC-DC-nucleosome complex. (**E**) Heat map showing particle orientation distribution. (**F**) Two views of the 10.60 Å resolution cryo-EM map of HDAC-DC-nucleosome complex with fitted coordinate. **(G)** Close-up views in stereo of the interface between the Hda2 NTD2 of one HDAC-PC and the Hda1 ARB2D of the other HDAC-PC fitted into 10.60 Å resolution cryo-EM map. **(H)** The 2D reprojection images (middle) of a modeled HDAC-DC-nucleosome complex (right) based on the experimental 2D classes (left) and the HDAC-DC-nucleosome 3D reconstruction.

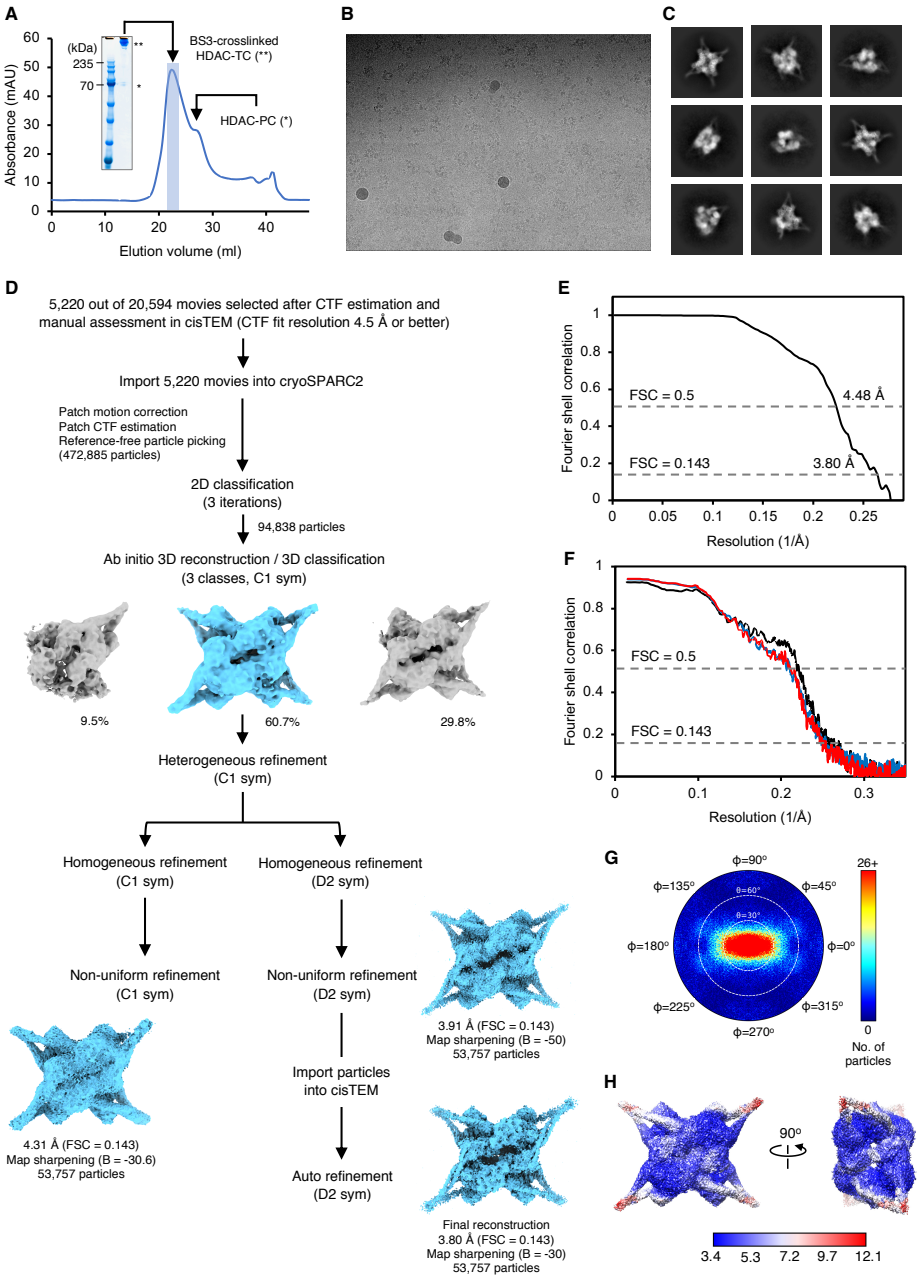

Fig. S10. Cryo-EM analysis of *S. cerevisiae* class II HDAC-TC. (**A**) SEC profile of BS3-crosslinked specimen on a gel filtration column (10/600 superose 6). SDS-PAGE of the selected fraction for preparing cryo-EM grids is shown. **(B)** Representative raw particles of HDAC-TC from an original micrograph. **(C)** Representative reference-free 2D class averages of HDAC-TC. **(D)** Summary of the image processing workflow. **(E)** Gold-standard FSC curve for the density map. The overall resolution is estimated at 3.80 Å (FSC = 0.143). **(F)** Model map FSC curve calculated between the refined atomic model and the half map used for refinement (blue, FSC_{work}), the second half-map not used in refinement (red, FSC_{test}) and the full map (black, FSC_{full}). **(G)** Heat map showing particle orientation distribution of HDAC-TC. **(H)** Local resolution represented by a heat map on the density contour of HDAC-TC (unsharpened, summed map).

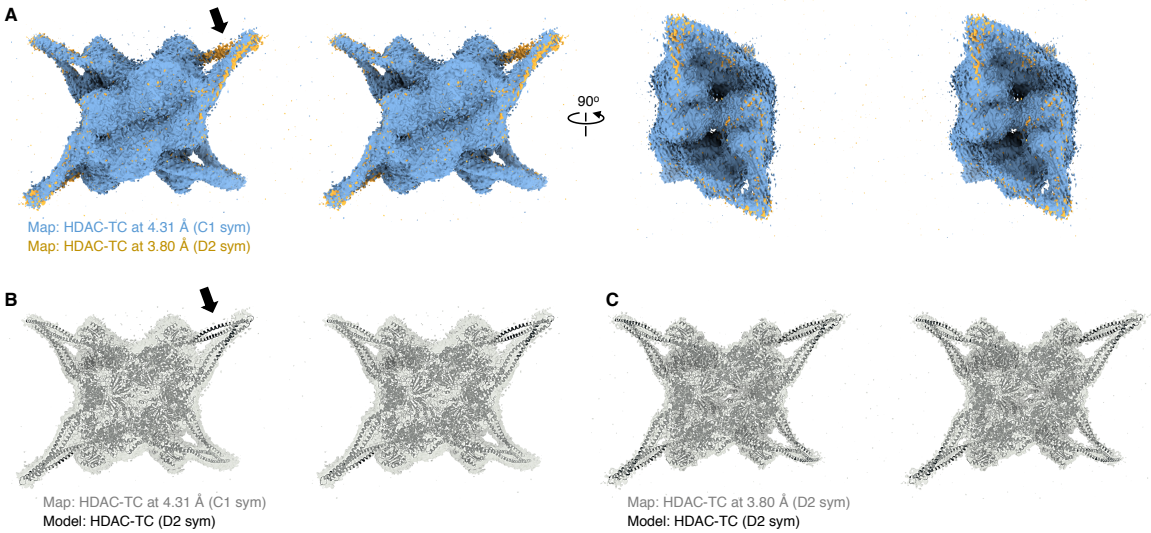

Fig. S11. Comparison of the HDAC-TC cryo-EM maps with and without imposed D2 symmetry. (**A**) Superposition in stereo of 4.31 Å resolution cryo-EM map (C1) with 3.80 Å resolution map with imposed D2 symmetry. The poor electron density of the C1 map corresponding to the Hda3 CCD3 in one protomer is indicated by arrow. **(B and C)** Superposition in stereo of the HDAC-TC structure with two individual cryo-EM maps.

Table S1. Cryo-EM data collection, refinement, and validation statistics

	HDAC-PC EMDB-11092 PDB 6Z6F	HDAC-DC EMDB-11094 PDB 6Z6H	HDAC-TC EMDB-11101 PDB 6Z6O	HDAC-PC-Nucleosome EMDB-11102 PDB 6Z6P	HDAC-DC-Nucleosome EMDB-11712
Data collection and processing					
Microscope	Glacios	Glacios	Titan Krios	Titan Krios	Glacios
Detector	K2	K2	K3	K3	K2
Magnification	36,000	22,000	105,000	105,000	22,000
Voltage (kV)	200	200	300	300	200
Electron exposure ($e^-/Å^2$)	62.1	62.0	86.0	77.2	60.8
Defocus range (μm)	1.0 - 2.5	1.5 - 3.0	0.8 - 3.2	0.6 - 2.4	1.5 - 3.0
Pixel size (Å)	1.181	1.885	0.8512	0.8512	1.885
Symmetry imposed	C1	C2	D2	C1	C1
Initial particle images (no.)	1,721,559	689,384	472,885	1,141,091	332,730
Final particle images (no.)	466,972	11,396	53,757	41,279	9,534
Map resolution (Å)	3.11	8.55	3.80	4.43	10.60
FSC threshold	0.143	0.143	0.143	0.143	0.143
Map resolution range (Å)	2.9 - 5.0	7.9 - 14.1	3.4 - 12.1	3.5 - 16.1	9.6 - 17.2
Map sharpening *B* factor ($Å^2$)	-77.1	-422.2	-30.0	-26.0	-450
Refinement					
Model resolution (Å)	3.0	9.1	4.0	4.5	
FSC threshold	0.143	0.143	0.143	0.143	
Initial model used (PDB code)	3HGT, 5J8J	HDAC-PC	HDAC-PC	HDAC-PC, 3LZ0	
Model composition					
Non-hydrogen atoms	19,217	38,434	77,516	31,115	
Protein residues	2,387	4,774	9,628	3,138	
Nucleotide residues	-	-	-	290	
Ligands	2	4	8	2	
R.m.s. deviations					
Bond lengths (Å)	0.006	0.009	0.006	0.010	
Bond angles (°)	1.020	1.593	0.925	1.617	
Validation					
MolProbity score	2.03	1.80	1.92	2.06	
Clashscore	3.62	6.40	7.98	9.57	
Poor rotamers (%)	3.55	0.25	0.96	1.29	
Ramachandran plot					
Favored (%)	92.82	92.92	92.11	92.49	
Allowed (%)	7.14	7.08	7.89	7.48	
Disallowed (%)	0.04	0.00	0.00	0.03	

REFERENCES AND NOTES

1. A. Inoue, D. Fujimoto, Enzymatic deacetylation of histone. *Biochem. Biophys. Res. Commun.* **36**, 146–150 (1969).
2. D. E. Ayer, Histone deacetylases: Transcriptional repression with SINers and NuRDs. *Trends Cell Biol.* **9**, 193–198 (1999).
3. S. E. Rundlett, A. A. Carmen, R. Kobayashi, S. Bavykin, B. M. Turner, M. Grunstein, Hda1 and Rpd3 are members of distinct yeast histone deacetylase complexes that regulate silencing and transcription. *Proc. Natl. Acad. Sci. U.S.A.* **93**, 14503–14508 (1996).
4. M. M. Kasten, S. Dorland, D. J. Stillman, A large protein complex containing the yeast Sin3p and Rpd3p transcriptional regulators. *Mol. Cell. Biol.* **17**, 4852–4858 (1997).
5. J. Wu, A. A. Carmen, R. Kobayashi, N. Suka, M. Grunstein, Hda2 and Hda3 are related proteins that interact with and are essential for the activity of the yeast histone deacetylase Hda1. *Proc. Natl. Acad. Sci. U.S.A.* **98**, 4391–4396 (2001).
6. J.-H. Lee, K. Maskos, R. Huber, Structural and functional studies of the yeast class II Hda1 histone deacetylase complex. *J. Mol. Biol.* **391**, 744–757 (2009).
7. J. Wu, N. Suka, M. Carlson, M. Grunstein, Tup1 utilizes histone H3/H2B-specific Hda1 deacetylase to repress gene activity in yeast. *Mol. Cell* **7**, 117–126 (2001).
8. S. D. Ha, S. Ham, M. Y. Kim, J. H. Kim, I. Jang, B. B. Lee, M. K. Lee, J.-T. Hwang, T.-Y. Roh, T. Kim, Transcription-dependent targeting of Hda1C to hyperactive genes mediates H4-specific deacetylation in yeast. *Nat. Commun.* **10**, 4270 (2019).
9. D. Robyr, Y. Suka, I. Xenarios, S. K. Kurdistani, A. Wang, N. Suka, M. Grunstein, Microarray deacetylation maps determine genome-wide functions for yeast histone deacetylases. *Cell* **109**, 437–446 (2002).
10. H. Shen, Y. Zhu, C. Wang, H. Yan, M. Teng, X. Li, Structural and histone binding ability characterization of the ARB2 domain of a histone deacetylase Hda1 from *Saccharomyces cerevisiae*. *Sci. Rep.* **6**, 33905 (2016).
11. G. Job, C. Brugger, T. Xu, B. R. Lowe, Y. Pfister, C. Qu, S. Shanker, J. I. Baños Sanz, J. F. Partridge, T. Schalch, SHREC silences heterochromatin via distinct remodeling and deacetylation modules. *Mol. Cell* **62**, 207–221 (2016).
12. J. D. Osko, D. W. Christianson, Structural basis of catalysis and inhibition of HDAC6 CD1, the enigmatic catalytic domain of histone deacetylase 6. *Biochemistry* **58**, 4912–4924 (2019).

13. N. J. Porter, A. Mahendran, R. Breslow, D. W. Christianson, Unusual zinc-binding mode of HDAC6-selective hydroxamate inhibitors. *Proc. Natl. Acad. Sci. U.S.A.* **114**, 13459–13464 (2017).
14. R. Marmorstein, Structure of histone deacetylases: Insights into substrate recognition and catalysis. *Structure* **9**, 1127–1133 (2001).
15. G. Hauk, G. D. Bowman, Structural insights into regulation and action of SWI2/SNF2 ATPases. *Curr. Opin. Struct. Biol.* **21**, 719–727 (2011).
16. L. Yan, Z. Chen, A unifying mechanism of DNA translocation underlying chromatin remodeling. *Trends Biochem. Sci.* **45**, 217–227 (2020).
17. D. Vasudevan, E. Y. D. Chua, C. A. Davey, Crystal structures of nucleosome core particles containing the '601′ strong positioning sequence. *J. Mol. Biol.* **403**, 1–10 (2010).
18. R. M. Lombardi, K. E. Cole, D. P. Dowling, D. W. Christianson, Structure, mechanism, and inhibition of histone deacetylases and related metalloenzymes. *Curr. Opin. Struct. Biol.* **21**, 735–743 (2011).
19. P. J. Watson, L. Fairall, G. M. Santos, J. W. R. Schwabe, Structure of HDAC3 bound to co-repressor and inositol tetraphosphate. *Nature* **481**, 335–340 (2012).
20. M. Arrar, R. Turnham, L. Pierce, C. A. F. de Oliviera, J. A. McCammon, Structural insight into the separate roles of inositol tetraphosphate and deacetylase-activating domain in activation of histone deacetylase 3. *Protein Sci.* **22**, 83–92 (2013).
21. N. J. Porter, N. H. Christianson, C. Decroos, D. W. Christianson, Structural and functional influence of the glycine-rich loop G^{302}GGGY on the catalytic tyrosine of histone deacetylase 8. *Biochemistry* **55**, 6718–6729 (2016).
22. C. J. Millard, P. J. Watson, I. Celardo, Y. Gordiyenko, S. M. Cowley, C. V. Robinson, L. Fairall, J. W. R. Schwabe, Class I HDACs share a common mechanism of regulation by inositol phosphates. *Mol. Cell* **51**, 57–67 (2013).
23. W.-M. Yang, S.-C. Tsai, Y.-D. Wen, G. Fejer, E. Seto, Functional domains of histone deacetylase-3. *J. Biol. Chem.* **277**, 9447–9454 (2002).
24. L. Guo, A. Han, D. L. Bates, J. Cao, L. Chen, Crystal structure of a conserved N-terminal domain of histone deacetylase 4 reveals functional insights into glutamine-rich domains. *Proc. Natl. Acad. Sci. U.S.A.* **104**, 4297–4302 (2007).

25. Y. Miyake, J. J. Keusch, L. Wang, M. Saito, D. Hess, X. Wang, B. J. Melancon, P. Helquist, H. Gut, P. Matthias, Structural insights into HDAC6 tubulin deacetylation and its selective inhibition. *Nat. Chem. Biol.* **12**, 748–754 (2016).
26. C. Hubbert, A. Guardiola, R. Shao, Y. Kawaguchi, A. Ito, A. Nixon, M. Yoshida, X.-F. Wang, T.-P. Yao, HDAC6 is a microtubule-associated deacetylase. *Nature* **417**, 455–458 (2002).
27. J. J. Kovacs, P. J. M. Murphy, S. Gaillard, X. Zhao, J.-T. Wu, C. V. Nicchitta, M. Yoshida, D. O. Toft, W. B. Pratt, T.-P. Yao, HDAC6 regulates Hsp90 acetylation and chaperone-dependent activation of glucocorticoid receptor. *Mol. Cell* **18**, 601–607 (2005).
28. Z. Wang, C. Zang, K. Cui, D. E. Schones, A. Barski, W. Peng, K. Zhao, Genome-wide mapping of HATs and HDACs reveals distinct functions in active and inactive genes. *Cell* **138**, 1019–1031 (2009).
29. N. Robbins, M. D. Leach, L. E. Cowen, Lysine deacetylases Hda1 and Rpd3 regulate Hsp90 function thereby governing fungal drug resistance. *Cell Rep.* **2**, 878–888 (2012).
30. P. L. Fidel Jr., J. A. Vazquez, J. D. Sobel, *Candida glabrata*: Review of epidemiology, pathogenesis, and clinical disease with comparison to *C. albicans*. *Clin. Microbiol. Rev.* **12**, 80–96 (1999).
31. N. A. R. Gow, F. L. van de Veerdonk, A. J. P. Brown, M. G. Netea, *Candida albicans* morphogenesis and host defence: Discriminating invasion from colonization. *Nat. Rev. Microbiol.* **10**, 112–122 (2011).
32. M. R. Peterson, R. J. Price, S. Gourlay, A. May, J. Tullet, A. Buscaino, The fungal-specific Hda2 and Hda3 proteins regulate morphological switches in the human fungal pathogen *Candida albicans*. bioRxiv 340364 [**Preprint**]. 7 June, 2018. https://doi.org/10.1101/340364.
33. K. Luger, T. J. Rechsteiner, T. J. Richmond, Expression and purification of recombinant histones and nucleosome reconstitution. *Methods Mol. Biol.* **119**, 1–16 (1999).
34. D. N. Mastronarde, Automated electron microscope tomography using robust prediction of specimen movements. *J. Struct. Biol*. **152**, 36–51 (2005).
35. A. Punjani, J. L. Rubinstein, D. J. Fleet, M. A. Brubaker, cryoSPARC: Algorithms for rapid unsupervised cryo-EM structure determination. *Nat. Methods* **14**, 290–296 (2017).
36. T. Grant, A. Rohou, N. Grigorieff, *cis*TEM, user-friendly software for single-particle image processing. *eLife* **7**, e35383 (2018).

37. E. F. Pettersen, T. D. Goddard, C. C. Huang, G. S. Couch, D. M. Greenblatt, E. C. Meng, T. E. Ferrin, UCSF Chimera—A visualization system for exploratory research and analysis. *J. Comput. Chem.* **25**, 1605–1612 (2004).
38. P. Emsley, K. Cowtan, *Coot*: Model-building tools for molecular graphics. *Acta. Crystallogr. D Biol. Crystallogr.* **60**, 2126–2132 (2004).
39. P. V. Afonine, B. K. Poon, R. J. Read, O. V. Sobolev, T. C. Terwilliger, A. Urzhumtsev, P. D. Adams, Real-space refinement in *PHENIX* for cryo-EM and crystallography. *Acta. Crystallogr. D Biol. Crystallogr.* **74**, 531–544 (2018).
40. V. B. Chen, W. B. Arendall III, J. J. Headd, D. A. Keedy, R. M. Immormino, G. J. Kapral, L. W. Murray, J. S. Richardson, D. C. Richardson, *MolProbity*: All-atom structure validation for macromolecular crystallography. *Acta. Crystallogr. D Biol. Crystallogr.* **66**, 12–21 (2010).
41. T. D. Goddard, C. C. Huang, E. C. Meng, E. F. Pettersen, G. S. Couch, J. H. Morris, T. E. Ferrin, UCSF ChimeraX: Meeting modern challenges in visualization and analysis. *Protein Sci*. **27**, 14–25 (2018).
42. Y. Hai, S. A. Shinsky, N. J. Porter, D. W. Christianson, Histone deacetylase 10 structure and molecular function as a polyamine deacetylase. *Nat. Commun.* **8**, 15368 (2017).
43. L. Farnung, S. M. Vos, C. Wigge, P. Cramer, Nucleosome-Chd1 structure and implications for chromatin remodelling. *Nature* **550**, 539–542 (2017).
44. M. Li, X. Xia, Y. Tian, Q. Jia, X. Liu, Y. Lu, M. Li, X. Li, Z. Chen, Mechanism of DNA translocation underlying chromatin remodelling by Snf2. *Nature* **567**, 409–413 (2019).
45. L. Yan, H. Wu, X. Li, N. Gao, Z. Chen, Structures of the ISWI-nucleosome complex reveal a conserved mechanism of chromatin remodeling. *Nat. Struct. Mol. Biol.* **26**, 258–266 (2019).